Ab Initio Fragment Molecular Orbital Study of Molecular Interactions between Liganded Retinoid X Receptor and Its Coactivator; Part II: Influence of Mutations in Transcriptional Activation Function 2 Activating Domain Core on the Molecular Interactions†

Mika Ito,*,‡,§ Kaori Fukuzawa,|| Yuji Mochizuki,§,⊥ Tatsuya Nakano,§,# and Shigenori Tanaka*,‡,§

Graduate School of Human Development and Environment, Kobe University, 3-11 Tsurukabuto, Nada, Kobe 657-8501, Japan, CREST, Japan Science and Technology Agency, Mizuho Information and Research Institute, Incorporated, 2-3 Kanda Nishiki-cho, Chiyoda-ku, Tokyo 101-8443, Japan, Department of Chemistry, Faculty of Science, Rikkyo University, 3-34-1 Nishi-Ikebukuro, Toshima-ku, Tokyo 171-8501, Japan, and Division of Safety Information on Drugs, Food, and Chemicals, National Institute of Health Sciences, 1-18-1 Kamiyoga, Setagaya-ku, Tokyo 158-8501, Japan

Received: July 11, 2007; In Final Form: September 3, 2007

The ab initio fragment molecular orbital (FMO) calculations were performed for retinoid X receptor (RXR) complexes with its ligand 9-cis retinoic acid (9cRA) and steroid receptor coactivator-1 (SRC1) to examine the influence of mutations in transcriptional activation function 2 activating domain core (AF2C) of RXR on molecular interactions between 9cRA liganded RXR and SRC1 coactivator. The RXR−SRC1 interactions in three types of RXR-9cRA-SRC1 complexes, namely, a wild type (WT), a mutant whose Glu453 of AF2C was substituted by Lys (E453K), and another mutant whose Glu456 of AF2C was substituted by Lys (E456K), were compared. Through the comparison of WT, E453K, and E456K, possible causes for a marked decrease in the transcriptional activity of RXR by the mutation of Glu453, which is known as a highly conserved charged residue of AF2C, were discussed. It was quantitatively demonstrated that the strength of the RXR−SRC1 interaction correlates with the degree of the transcriptional activation (WT > E456K > E453K). In E453K, the RXR−SRC1 interaction was substantially reduced by the AF2C−SRC1 repulsive interaction, and the charge transfer (CT) from RXR to SRC1 was also inhibited by the decreased electron donation from AF2C to SRC1. Our findings suggest that the inhibitions of the local RXR−SRC1 interaction via AF2C and of the local CT from RXR to SRC1 via AF2C would be the possible causes for the marked decrease in the transcriptional activity of RXR.

1. Introduction

The retinoid X receptor (RXR) is a member of the nuclear receptor (NR) superfamily and acts as a ligand-inducible transcriptional regulator that regulates expression of many genes involved in various physiological actions of its ligands at the transcriptional level. Its natural ligand 9-*cis* retinoic acid (9cRA) is the metabolite of vitamin A that controls morphogenesis, differentiation, and homeostasis during embryonal development and postnatal life. 9cRA is also an effective inhibitor of tumor cell growth, and this antitumor activity is useful in therapy and prevention of cancers such as human immunodeficiency virus (HIV) associated Kaposi's sarcoma.[1,2] RXR not only forms a homodimeric DNA complex, but also can form heterodimeric DNA complexes with various NRs, such as retinoic acid receptor (RAR), thyroid hormone receptor (TR), vitamin D receptor (VDR), and peroxisome proliferator-activated receptor (PPAR).[3] Because RXR has diverse important biological roles associated with human life and diseases, it has been one of the primary targets of drug discovery.

To date, many experimental studies have been devoted to elucidate the transcriptional activation mechanism of RXR so as to efficiently exploit the functions of RXR. It is now widely accepted that the transcriptional activity of RXR, as well as many NRs, is induced by the binding of a ligand to RXR ligand-binding domain (LBD), which contains the ligand-dependent transcriptional activation function 2 (AF-2), and controlled by the exchange of the binding of transcriptional coregulators including coactivator and corepressor to RXR LBD.[4]

From comparison of the X-ray crystal structures of human RXRα (hRXRα) *apo*-LBD[5] and hRARγ *holo*-LBD,[6] an early experimental study[6] proposed a "mouse trap" mechanism that involves ligand-induced remarkable conformational changes of NR LBD especially in the configuration of a C-terminal helix 12 (H12) for the transcriptional activation mechanism and identified that the repositioned H12 contains the AF-2 activating domain core (AF2C) which is thought to be crucial in mediating the ligand-dependent transcriptional activation of NRs. This model mechanism was subsequently validated by comparison of hRXRα *apo*-LBD[5] and hRXRα *holo*-LBD.[7] On the basis of these experimental studies, H12 was proposed as a ligand-

† Part of the "William A. Lester, Jr., Festschrift".

* To whom correspondence should be addressed. Phone: +81-78-803-7991. Fax: +81-78-803-7761. E-mail: ito@insilico.h.kobe-u.ac.jp (M.I.), tanaka2@kobe-u.ac.jp (S.T.).

‡ Kobe University.

§ Japan Science and Technology Agency.

|| Mizuho Information and Research Institute, Incorporated.

⊥ Rikkyo University.

National Institute of Health Sciences.

10.1021/jp075430r CCC: $40.75
Published on Web 11/17/2007

Figure 1. Ribbon display of the X-ray crystal structure (PDB code 1FM9) of the hRXRα LBD (green) complexed with 9cRA (purple) and SRC1 peptide (blue). The position of AF2C (red) in H12 is also displayed.

hRXRα	450	F	L	M	E	M	L	E
mRXRβ	436	F	L	M	E	M	L	E
hRARα	409	L	I	Q	E	M	L	E
hRARγ	411	L	I	R	E	M	L	E
hTRβ	454	L	F	L	E	V	F	E
hVDR	417	L	V	L	E	V	F	G
hPPARγ	468	L	L	Q	E	I	Y	K
hERα	539	L	L	L	E	M	L	D

Figure 2. Sequence alignment of AF2C in hRXRα with the corresponding region in NRs. The names of NRs, residue numbers of the first amino acid residue in AF2C, and amino acid sequences of AF2C are displayed from left to right. Highly conserved charged residues are in red box.

dependent "switch" of the transcriptional activation mechanism, which generates the surface for coactivator binding or recognition in its ligand-induced functional configuration.[8]

Afterward, structural studies[9,10] of NR LBD complexes with its ligands and coactivators such as steroid receptor coactivator-1 (SRC1) reported that a helical LXXLL motif of a coactivator makes contacts with the surface of NR LBD, where a "charge clamp" composed of lysine and glutamate residues in H3 and H12 of NR LBD, respectively, forms hydrogen bonds with backbone atoms of the LXXLL motif of a coactivator. The same structural character was also identified in the X-ray crystal structures of the hRXRα LBD complex with 9cRA and SRC1 (Figure 1),[11] and Lys284 in H3 and Glu453 of AF2C in H12 were identified as the residues that form the "charge clamp".[11,12] These structural data suggested that a particular position of H12 is essential to support coactivator binding.

It is now well-known that, among many NRs, H12 has a conserved motif[13] referred to as AF2C including a highly conserved charged residue[14−20] that forms the "charge clamp" (Figure 2). Figure 2 shows the sequence alignment of AF2C in hRXRα with the corresponding region in human (h) or mouse (m) NRs such as RAR, TR, VDR, PPAR, and estrogen receptor (ER). As shown in Figure 2, the conserved motif of hRXRα is formed by seven amino acids including two charged residues Glu453 and Glu456 (E in a single-letter abbreviation), and the highly conserved charged residue of hRXRα is Glu453. Biological studies on NRs[14−19] have shown that a mutation of the highly conserved charged residue in AF2C impaired coactivator binding and markedly reduced transcriptional activity of NRs. These studies suggested the marked decrease in transcriptional activity of NRs would be due to the inhibition of coactivator binding. In addition, a biological study on RXR[20] has shown that all mutations of five selected residues in AF2C reduced transcriptional activity of RXR, and a mutation of Glu453 led to the highest decrease in the transcriptional activity. It is noteworthy that a mutation of the highly conserved charged residue Glu453 to Lys (E453K) has a larger effect on the reduction of transcriptional activity of RXR than a similar mutation of another charged residue Glu456 to Lys (E456K). In spite of many experimental reports on the fact that the transcriptional activity of NRs is markedly decreased by the mutation of the highly conserved charged residue, precise causes of the fact remain unclear. To eventually understand the transcriptional activation mechanism of RXR, the precise causes for the fact that transcriptional activity of RXR is markedly decreased by the mutation of the highly conserved charged residue Glu453 should be clarified. In order to address this issue, detailed and accurate analysis of the coactivator binging mechanism and molecular interactions between RXR and coactivator are required.

By taking advantage of ab initio quantum mechanical (QM) calculations, we can perform detailed and accurate analysis of molecular interactions and charge transfers (CTs) as well as molecular structures and properties including charge redistributions, which cannot be described by classical molecular mechanical (MM) methods. Moreover, by using the fragment molecular orbital (FMO) method,[21−26] we can perform the ab initio QM calculations of bio-macromolecules, though the conventional molecular orbital (MO) method is limited to the ab initio QM calculations of small molecules. In particular, using the inter-fragment interaction energies (IFIEs)[27−30] evaluated by the FMO calculations, we can estimate molecular interactions at the residue level when the fragmentations are performed according to the amino acid unit for the protein. In addition, by means of electron-correlation methods beyond the Hartree−Fock (HF) method such as the second-order Møller-Plesset perturbation (MP2) method[31,32] with the FMO procedure, we can also appropriately describe the dispersion energies, which are known to be important for interactions in bio-macromolecules.[30,33]

In our previous study,[33] we have performed QM calculations for a wild type RXR-9cRA-SRC1 complex by the ab initio FMO method at the HF and MP2 levels using an X-ray crystal structure. We demonstrated that H12 and its highly conserved residues significantly contribute to the coactivator binding not only by electrostatic and dispersion interactions but also by a CT from RXR to SRC1. We found that the highly conserved charged residue Glu453 has a stronger interaction with SRC1 than the other residues in H12 of RXR. We also found that large positive and negative charges are induced on Glu453 of RXR and Lys631 and Ile632 of SRC1, respectively, suggesting that the highly conserved charged residue Glu453 may have an important role as an electron donor for Lys631 and Ile632 of SRC1 on the CT from RXR to SRC1. From our previous results, it was presumed that, if Glu453 was mutated, the coactivator binding would be impaired because of the decreased interaction and CT between RXR and SRC1. In addition, a previous QM

calculation[29] for ER complex with several ligands by the ab initio FMO method has shown that ligand binding energies are related to CTs from ER to ligands. In a recent QM calculation[30] with the ab initio FMO, CT interactions between ER and its natural ligand 17β-estradiol (EST) have been analyzed in detail on the basis of the configuration analysis for fragment interaction (CAFI)[34,35] method, and it was shown that the CT interactions could be a major controlling factor of ER-ligand binding. Therefore, it was supposed that the CT interactions between RXR and SRC1 are also important for their binding. To better understand the details of the transcriptional activation mechanism of RXR, it would be necessary to perform detailed and accurate analysis of CT interactions as well as electrostatic and dispersion interactions between SRC1 and individual amino acid residues of RXR, in comparison of mutant RXR-9cRA-SRC1 complexes with a wild type RXR-9cRA-SRC1 complex.

In the present study, in an effort to provide insight into the detailed molecular mechanism of the transcriptional activation of RXR, we have attempted to clarify what are the causes for the marked decrease in the transcriptional activity of hRXRα by the mutation of the highly conserved charged residue Glu453 of AF2C. To address this question, we have examined the influence of mutations in AF2C of hRXRα LBD on molecular interactions between 9cRA liganded hRXRα LBD and SRC1 coactivator at the residue level by the ab initio FMO calculations using the MP2 method. In this investigation, the RXR−SRC1 interactions in three types of RXR-9cRA-SRC1 complexes, namely, a wild type (WT), a mutant whose Glu453 of AF2C was substituted by Lys (E453K), and another mutant whose Glu456 of AF2C was substituted by Lys (E456K), were particularly focused on and compared with each other. In addition, CTs in the three types of RXR-9cRA-SRC1 complexes were also analyzed.

2. Theoretical Calculations

In our previous work,[33] the molecular interactions and CTs in a wild type RXR-9cRA-SRC1 complex were analyzed in detail using an X-ray crystal structure. In this work, the molecular interactions and CTs in three types of RXR-9cRA-SRC1 complexes, namely, WT, E453K, and E456K, were compared. Because X-ray crystal structures of E453K and E456K have not been reported, the structures of E453K and E456K were prepared by the molecular dynamics (MD) simulations and the geometry optimizations using MM methods in aqueous solution. In order to compare properties of WT, E453K, and E456K under the same conditions, the structures of WT, E453K, and E456K were prepared by similar MD simulations and MM geometry optimizations in aqueous solution. Using these structures, the ab initio FMO calculations were carried out for WT, E453K, and E456K under gas-phase conditions, because the ab initio FMO calculations including numerous water molecules in aqueous solution are difficult to perform at present. However, previous FMO calculations[29,30,33] under gas-phase conditions have provided much valuable information on molecular interactions and CTs in bio-macromolecules using X-ray crystal structures. The structures of WT, E453K, and E456K were prepared as described below.

2.1. Preparation of Molecular Structures. The initial atomic coordinates of WT were obtained from the Research Collaboratory for Structural Bioinformatics (RCSB) Protein Data Bank (PDB),[36] PDB code 1FM9 (Figure 1).[11] The entire hRXRα LBD consisting of 232 amino acid residues (residues 227−458), 9cRA, and SRC1 peptide consisting of 10 amino acid residues (residues 630−639) were employed for simulations. Missing hydrogen atoms and side chains in the PDB file were complemented manually by using the molecular graphic software Molecular Operating Environment (MOE), Version 2006.08.[37] Hydrogen atoms were added to both N- and C-terminal residues of the peptide chains and all of the dissociative and associative residues in their charged states. All of the positions of hydrogen atoms and side chains added in the procedure above were geometrically optimized under gas-phase conditions by using the AMBER99 force field[38] with the other heavy atoms fixed at the positions given in the PDB data. The initial atomic coordinates of E453K and E456K were obtained from WT prepared as described above. For E453K and E456K, Glu453 and Glu456, respectively, were substituted by lysine by using the molecular graphic software MOE. The positions of substituted residues were geometrically optimized under gas-phase conditions by using the AMBER99 force field.[38] The total numbers of atoms in WT, E453K, and E456K are 3926, 3933, and 3933, respectively, including hydrogen atoms. The charges of RXR in the WT, E453K, and E456K complexes are 0*e*, +2*e*, and +2*e*, respectively. The charges of 9cRA and SRC1 are −1*e* and +3*e*, respectively. The total charges of WT, E453K, and E456K are +2*e*, +4*e*, and +4*e*, respectively.

The MM and MD calculations for WT, E453K, and E456K were performed with the Amber7 program[39] on Intel Pentium 3.0 GHz (4 CPUs). Energy minimizations were performed by the steepest descent (SD) and the conjugate gradient (CG) methods. The AMBER99 force field[38] was used to parametrize RXR and SRC1. The charges of 9cRA were obtained after geometry optimization and subsequent single-point calculation of electrostatic potential at the Hartree−Fock (HF) level with the 6-31G(d) basis set by using the Gaussian03 program,[40] and were fitted by using the restrained electrostatic potential (RESP) procedure.[41,42] These force field parameters of 9cRA were assigned on the basis of the atom types of the force field model developed by Cornell et al.[43] By employing the initial atomic coordinates prepared above, the atomic coordinates of WT, E453K, and E456K were built using the LEaP module of the Amber7 program. After the coordination and energy minimization of hydrogen atoms, each complex was solvated in a rectangular box of TIP3P water molecules[44] with a minimum solute−wall distance of 10 Å and neutralized by adding chloride counterions.

The following procedures were performed for each solvated WT, E453K, and E456K by using the Sander module of the Amber7 program under the periodic boundary condition. The solvated system was optimized prior to the MD simulation through two steps. At the first step, the RXR-9cRA-SRC1 complex was frozen, and the solvent water molecules and chloride counterions were optimized by 500 steps of the SD energy minimization followed by 500 steps of the CG energy minimization. At the second step, the entire solvated system was optimized by 500 steps of the SD energy minimization followed by 500 steps of the CG energy minimization. The optimized system was gradually heated from 0 to 300 K within 20 ps by a constant volume MD simulation. A harmonic restraint of 10 kcal/mol/Å^2 was imposed on solutes while heating the system. Then, a production MD simulation was carried out for 1 ns under a periodic boundary condition in the NPT ensemble at constant pressure (1 atm) with isotropic position scaling and at 300 K with the Berendsen temperature coupling (using a time constant of 0.5 ps for heat bath coupling).[45] No harmonic restraints were imposed during the production MD simulation. The SHAKE algorithm was applied to fix all covalent bonds

containing a hydrogen atom.[46,47] The particle mesh Ewald (PME) method[48] was used to treat the long-range electrostatic interactions. A cutoff of 8 Å was applied to the noncovalent interactions, and a time step of 2 fs was used. During the 1 ns production MD simulation, the coordinates of the simulated complex were saved every 1 ps. The root-mean-squared deviation (RMSD) measurements of WT, E453K, and E456K along the simulation time are available as Supporting Information. The RMSD measurements show that each structure of WT, E453K, and E456K was structurally relaxed or equilibrated by the MD simulation.

For the FMO calculations, snapshots of equilibrated structures were taken from the last 201 ps (800 ps, 900 ps, and 1 ns) of the 1 ns production MD simulation. Each snapshot was annealed prior to the FMO calculations by the following procedures. The system was gradually cooled from 300 to 0 K within 20 ps by a constant volume MD simulation. A harmonic restraint of 10 kcal/mol/Å^2 was imposed on solutes while cooling the system. Then, the system was optimized by 2 ps of quenched dynamics (at a time step of 0.2 fs and at 0.1 K), followed by the CG energy minimization until the threshold energy decreased to less than 0.1 kcal/mol.

2.2. FMO Calculations. Each geometry of the RXR-9cRA-SRC1 complexes (WT, E453K, and E456K) used for the ab initio FMO[21−26] calculations was prepared by the procedure mentioned above, and the geometries of the RXR-9cRA complex and free SRC1 were fixed at the geometry of the RXR-9cRA-SRC1 complex. The ab initio FMO calculations were carried out under gas-phase conditions at the MP2 level[31,32] with the 6-31G basis set. The results of the ab initio FMO calculations for the snapshots of the MD simulations at 1 ns, 900 ps, and 800 ps respectively are shown as samples 1, 2, and 3 in tables of the following sections, and those for the X-ray crystal structure of WT, which was employed in our previous work,[33] are also shown as sample 0 to confirm the reliability of properties of WT prepared by the MD simulation. Additionally, the ab initio FMO calculations using modified MP2 methods such as the spin-component scaled MP2 (SCS-MP2)[49] method and the scaled opposite-spin MP2 (SOS-MP2)[50] method were also carried out for the snapshots of the MD simulations at 1 ns (sample 1) to assess the description of molecular energies, since the canonical MP2 method is known to consistently overestimate binding energies. These modified MP2 methods were recently implemented in our calculation program ABINIT-MP.[51]

To save computational time without losing significant accuracy, the approximations of electrostatic potentials considered as the Mulliken orbital charge (esp-aoc) and the fractional point charge (esp-ptc) were applied to fragments whose separations of the closest contact atoms were more than 0.0 and 2.0 in units of van der Waals (vdW) radii, respectively.[24] The Coulomb interaction approximation (dimer-es) was also applied to fragments whose separation was more than 2.0 in vdW units. The fragmentation was performed according to the amino acid unit for the protein, and each amino acid residue of RXR and SRC1 and the 9cRA molecule were treated as a single fragment. The number of fragments in the RXR-9cRA-SRC1 complex is 243.

The IFIE[27−30] in FMO calculations is defined as follows,

$$\Delta E_{IJ} = (E'_{IJ} - E'_I - E'_J) + Tr(\Delta \mathbf{P}^{IJ}\mathbf{V}^{IJ}) \qquad (1)$$

where $\Delta\mathbf{P}^{IJ}$ is a difference density matrix, $\mathbf{V}^{IJ}$ is an environmental electrostatic potential for fragment dimer IJ from other fragments, and E'_I and E'_{IJ} are energies of fragment monomer I and dimer IJ without environmental electrostatic potential. The many-body effects are considered through the environmental electrostatic potentials. From ΔE_{IJ}, the total energy E is calculated by

$$E = \sum_{I>J} \Delta E_{IJ} + \sum_I E'_I \qquad (2)$$

The IFIEs in the RXR-9cRA-SRC1 complex were analyzed primarily for the interactions between the residues of AF2C and SRC1. The IFIEs of the N- and C-terminal residues of RXR and SRC1 with the other residues are not listed in the tables of the following sections, because these residues are not ends of the peptide chains in the actual system.

All of the FMO calculations were performed with the ABINIT-MP program[51] on 32 Dual AMD Opteron 2.0 GHz clusters (64 CPUs), and the visualization was carried out with the BioStation Viewer.[52]

2.3. Binding Free Energy Calculations. The effects of solvent and entropy on coactivator binding affinities were estimated by the MM calculations using the AMBER99 force field,[38] because the ab initio QM calculations for free energies of bio-macromolecules by the FMO method are not available at present. The binding free energies (ΔG) of the RXR-9cRA-SRC1 complexes (WT, E453K, and E456K) in aqueous solution were calculated by the MM-GBSA (molecular mechanics-generalized Born[53] surface area[54]) method implemented in Amber. The MM-GBSA calculations usually give a reasonable estimate on the relative binding free energy,[55] though they may overestimate the absolute binding free energy because of the missing terms such as conformational entropy change of the solute upon binding. The binding free energies (ΔG) in aqueous solution calculated by the MM-GBSA method were compared with the binding energies (ΔE) calculated under gas-phase conditions by the MM method. The MM calculations of the binding energies were performed with the Amber8 program[56] on Intel Pentium 3.2 GHz (4 CPUs).

3. Results and Discussion

3.1. Structural Features. At the beginning of this investigation, the structural features of WT, E453K, and E456K were analyzed. Similar structures were obtained from the snapshots at 1 ns, 900 ps, and 800 ps (samples 1, 2, and 3) of the MD simulations for WT, E453K, and E456K. Figure 3a−c shows the structures of WT, E453K, and E456K obtained from the snapshots at 1 ns (sample 1). The distances between some residues in RXR and SRC1 of samples 1, 2, and 3 were calculated, and the average values of the distances calculated for WT, E453K, and E456K are compared below.

Figure 3a shows that the side chains of Lys284 and Glu453 of the "charge clamp" of WT form hydrogen bonds with the backbone carbonyl and amide of LXXLL motif of SRC1 with the calculated average distances r_1(H^{Lys284}−O^{Leu636}) and r_2-(O^{Glu453}−H^{Leu633}) of 1.95 and 2.07 Å, respectively, while these distances calculated for the X-ray crystal structure of WT are 1.83 and 2.02 Å, respectively. The observed structural feature of WT is in agreement with the experimental report.[9] It is shown that the Lys284−Leu636 and Glu453−Leu633 hydrogen bonds in WT are kept before and after the MD simulation.

On the one hand, in E453K, the substituted residue Lys453 does not have a hydrogen bond with Leu633, though the Lys284−Leu636 hydrogen bond is kept with the calculated average distance r_1(H^{Lys284}−O^{Leu636}) of 1.86 Å as shown in Figure 3b. In addition, the average distance r_4($C\alpha^{Lys453}$−$C\alpha^{Leu633}$) in E453K is longer than the average distance r_4-($C\alpha^{Glu453}$−$C\alpha^{Leu633}$) in WT by 3.37 Å. On the other hand, in

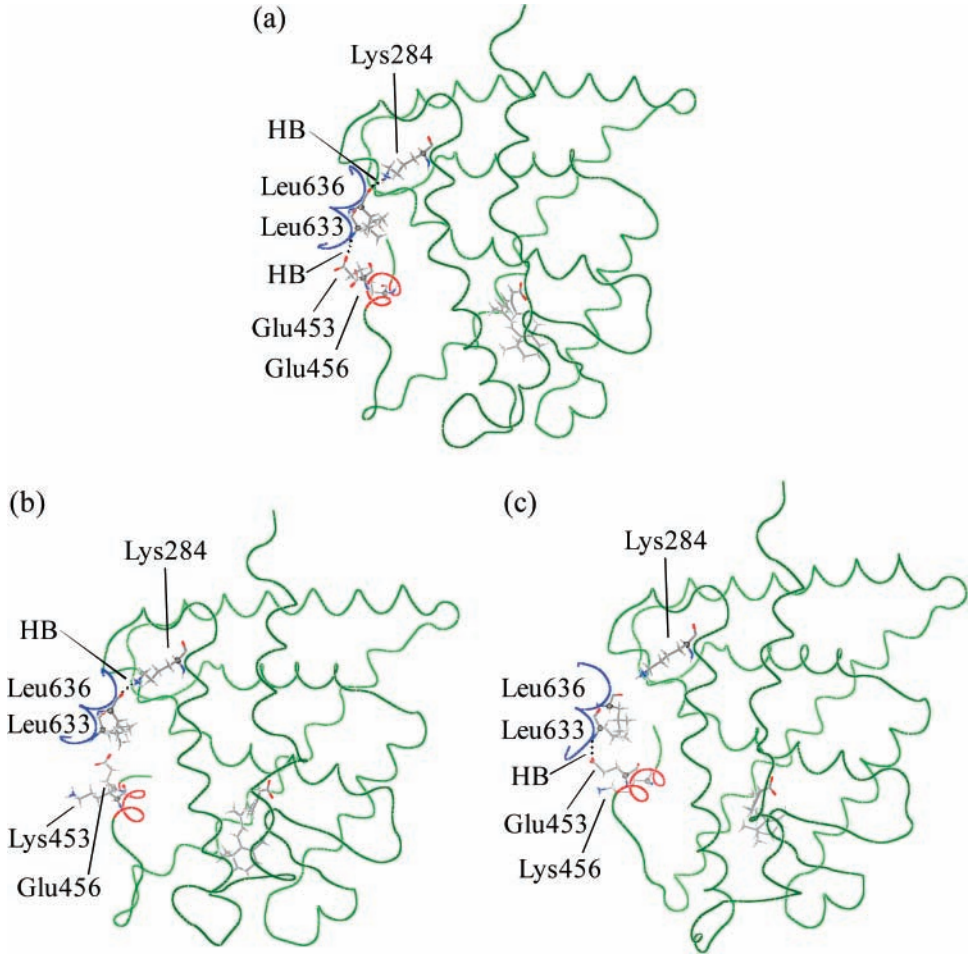

Figure 3. Ribbon display of (a) WT, (b) E453K, and (c) E456K of the RXR-9cRA-SRC1 complex model obtained from the snapshots at 1 ns of the MD simulations. RXR, AF2C, and SRC1 are displayed by green, red, and blue ribbons, respectively. The positions of hydrogen bonds (HB) and Cα atoms of displayed residues are shown by dotted lines and gray balls, respectively.

E456K, Lys284 does not have a hydrogen bond with Leu636, though the Glu453−Leu633 hydrogen bond is kept with the calculated average distance $r_2(O^{Glu453}-H^{Leu633})$ of 2.02 Å as shown in Figure 3c. Additionally, the average distance r_2-$(C\alpha^{Lys284}-C\alpha^{Leu636})$ in E456K is longer than that in WT by 2.09 Å. It is shown that the mutation of Glu453 in AF2C directly influences conformations of the amino acid residues which are situated near Glu453, whereas the mutation of Glu456 in AF2C indirectly influences conformations of the amino acid residues which are situated near Lys284.

3.2. Coactivator Binding Energies. To investigate the influence of mutations in AF2C on the SRC1 coactivator binding, the SRC1 coactivator binding energies of WT, E453K, and E456K were calculated by the FMO method at the MP2/6-31G level as shown in Table 1. The coactivator binding energy (ΔE) is given as follows,

$$\Delta E = E(\mathrm{RLC}) - [E(\mathrm{RL}) + E(\mathrm{C})] \qquad (3)$$

where E(RLC), E(RL), and E(C) are the total energies of the receptor−ligand−coactivator complex (RLC), the receptor−ligand complex (RL), and the coactivator (C), respectively. The averages and standard deviations were also calculated for the SRC1 binding energies of the three snapshots (at 1 ns, 900 ps, and 800 ps) of the MD simulations. Note that the calculated coactivator binding energies are perhaps too large to be considered literally. In a previous theoretical study[57] on ligand binding affinity for ER by MD simulations, it has been shown that, though the binding energies of various ligands calculated without the effects of solvent and entropy are larger than those calculated with the effects of solvent and entropy or derived from experiments by about 50 kcal/mol, the tendency of the former ligand binding affinities is consistent with that of the latter ligand binding affinities. On the basis of this previous theoretical estimation, it is suggested that, if the effects of solvent and entropy are included in the calculations, the coactivator binding energies for RXR would be substantially reduced, but the qualitative tendency of the coactivator binding affinities for RXR would not be changed. In addition, the basis set superposition error (BSSE) could be one of the reasons for the overestimation of the binding energies, though the effect of BSSE for the binding energies would be smaller than the effects of solvent and entropy. Previous theoretical studies[58,59] on binding energies of several nucleic acid base pairs have shown that, though the binding energies calculated at the MP2/6-31G level were overestimated by about 20% compared with the values including the BSSE corrections calculated at the MP2/cc-pVTZ level, the tendency of the former binding affinities is consistent with that of the latter binding affinities. Therefore, the qualitative tendency of the coactivator binding affinities for RXR estimated at the MP2/6-31G level would not be changed by BSSE.

In order to confirm the validity of the canonical MP2 calculation for the coactivator binding energies, the SCS-MP2 and SOS-MP2 calculations for the binding energies were also performed using sample 1. The magnitudes of the SRC1 binding energies calculated for sample 1 are in order of WT > E456K

TABLE 1: Coactivator Binding Energies (Δ*E*) and Binging Free Energies (Δ*G*) Calculated for WT, E453K, and E456K[a]

energy	method	sample		WT	E453K	E456K
Δ*E*	FMO	0	crystal structure	−586.95		
		1	MD 1 ns	−630.84	−252.63	−337.89
		2	MD 900 ps	−622.34	−274.99	−300.25
		3	MD 800 ps	−659.01	−334.29	−256.17
		1−3	average[b]	−637.40	−287.30	−298.10
		1−3	standard deviation[c]	15.67	34.46	33.40
	MM	1	MD 1 ns	−670.58	−239.26	−386.93
		2	MD 900 ps	−661.57	−272.37	−332.02
		3	MD 800 ps	−714.07	−330.08	−282.75
		1−3	average[b]	−682.07	−280.57	−333.90
		1−3	standard deviation[c]	22.92	37.53	42.55
Δ*G*	MM-GBSA	1	MD 1 ns	−51.90	−26.28	−34.50
		2	MD 900 ps	−55.43	−26.92	−30.89
		3	MD 800 ps	−47.45	−34.15	−32.34
		1−3	average[b]	−51.59	−29.12	−32.58
		1−3	standard deviation[c]	3.27	3.57	1.48

[a] $\Delta E = E(\mathrm{RLC}) - [E(\mathrm{RL}) + E(\mathrm{C})]$, where E(RLC), E(RL), and E(C) are the total energies of the receptor−ligand−coactivator complex (RLC), the receptor−ligand complex (RL), and the coactivator (C), respectively. $\Delta G = G(\mathrm{RLC}) - [G(\mathrm{RL}) + G(\mathrm{C})]$, where G(RLC), G(RL), and G(C) are the total free energies of RLC, RL, and C, respectively. Binding energies (Δ*E* in kcal/mol) are calculated under gas-phase conditions by the FMO method at the MP2/6-31G level or by the MM method, and corresponding binding free energies (Δ*G* in kcal/mol) in aqueous solutions are calculated by the MM-GBSA method. [b] Average of the samples 1−3. [c] Standard deviation of the samples 1−3.

> E453K with the calculated values of −630.8, −337.9, and −252.6 kcal/mol at the MP2/6-31G level, respectively. By the SCS-MP2 and SOC-MP2 calculations, the magnitudes of the binding energies of sample 1 are also in order of WT > E456K > E453K with the calculated values of −618.6, −328.7, and −244.4 kcal/mol at the SCS-MP2/6-31G level and −612.5, −324.1, and −240.3 kcal/mol at the SOS-MP2/6-31G level, respectively. It was shown that the tendency of the strength of SRC1 binding estimated by the canonical MP2 method was similar to that estimated by the SCS-MP2 and SOS-MP2 methods, though the binding energies were somewhat overestimated by the canonical MP2 method. Hence, the following discussions are based on the results obtained by the canonical MP2 calculations.

As shown in Table 1, the average magnitude of the coactivator binding energy of WT prepared by the MD simulation is somewhat larger than that of WT of the X-ray crystal structure, possibly because of the difference in the equilibrated and non-equilibrated structures of WT. The significant differences of these structures are observed in the configurations of the N- and C-terminals (His630 and Glu639, respectively) of SRC1 whose backbone amino and carbonyl are prepared in their charged states. For example, the average Cα-Cα distance (5.83 Å) between the N-terminal residue His630 of SRC1 and the "charge clamp" residue Glu453 of RXR in equilibrated WT (samples 1, 2, and 3) is shorter than that (6.69 Å) in non-equilibrated WT (sample 0) by 0.86 Å, and the average Cα-Cα distance (9.44 Å) between the C-terminal residue Glu639 of SRC1 and the "charge clamp" residue Lys284 of RXR in equilibrated WT (samples 1, 2, and 3) is shorter than that (10.47 Å) in non-equilibrated WT (sample 0) by 1.03 Å. Additionally, the main chain atoms of His630 and Glu639 are vicinal to the side chain atoms of Glu453 and Lys284, respectively, and the average distance (3.64 Å) between the main chain carbonyl C atom of Glu639 and the side chain amino N atom of Lys284 in equilibrated WT (samples 1, 2, and 3) is shorter than that (4.54 Å) in non-equilibrated WT (sample 0) by 0.90 Å, while the average distance (5.06 Å) between the main chain amino N atom of His630 and the side chain carbonyl C atom of Glu453 in equilibrated WT (samples 1, 2, and 3) is almost equal to that (5.07 Å) in non-equilibrated WT (sample 0).

The results of the FMO calculations (Table 1) show that the average of the absolute values of the SRC1 binding energies (Δ*E*) of WT is larger than that of E453K and E456K by 350.1 and 339.3 kcal/mol, respectively, and the magnitudes of the averages of the binding energies are in order of WT > E456K > E453K. The standard deviation of the SRC1 binding energies of WT is small compared with the binding energies themselves. In addition, the standard deviation of the SRC1 binding energies of WT is smaller than that of E453K and E456K by 18.8 and 17.7 kcal/mol, respectively, and the standard deviations of the binding energies are in order of WT < E456K < E453K. These results show that SRC coactivator binds to 9cRA liganded RXR in the WT complex more strongly than in the E453K and E456K complexes. From these results, it is indicated that the average strength of SRC1 binding correlates with the degree of the transcriptional activation (WT > E456K > E453K), which was reported in an experimental study.[20]

Although the effects of solvent and entropy on the coactivator binding affinities cannot be evaluated by the FMO calculations at present, they can be estimated by the MM calculations. In order to estimate these effects, the binding energy (Δ*E*) in gas phase and corresponding binding free energies (Δ*G*) in aqueous solution were also calculated by the MM and MM-GBSA methods, respectively, as shown in Table 1. The coactivator binding free energy (Δ*G*) is given as follows,

$$\Delta G = G(\mathrm{RLC}) - [G(\mathrm{RL}) + G(\mathrm{C})] \qquad (4)$$

where G(RLC), G(RL), and G(C) are the total free energies of the receptor−ligand−coactivator complex (RLC), the receptor−ligand complex (RL), and the coactivator (C), respectively.

The results of the MM calculations (Table 1) show that the average of the absolute values of the SRC1 binding energies (Δ*E*) of WT is larger than that of E453K and E456K by 401.5 and 348.2 kcal/mol, respectively. Both the FMO and MM calculations show that the magnitudes of the averages of the binding energies (Δ*E*) are in order of WT > E456K > E453K with the calculated values of −637.4, −298.1, and −287.3 kcal/mol, respectively, by the FMO method and of −682.1, −333.9, and −280.6 kcal/mol, respectively, by the MM method, though these SRC1 binding energies above are perhaps too large to be considered literally. On the other hand, the results of the MM calculations show that the magnitudes of the averages of the binding free energies (Δ*G*) are also in order of WT > E456K > E453K with the calculated values of −51.6, −32.6, and −29.1

TABLE 2: IFIEs[a] of the Whole RXR or Its AF2C with the Whole SRC1 or Its LXXLL Motif Calculated for WT, E453K, and E456K

sample		interaction	WT	E453K	E456K
0	crystal structure	INT1	−365.40		
		INT2	−302.14		
		INT3	−188.50		
1	MD 1 ns	INT1	−364.17	−57.96	−199.60
		INT2	−300.72	18.00	−113.09
		INT3	−178.87	7.72	−61.60
2	MD 900 ps	INT1	−338.38	−49.52	−177.80
		INT2	−279.39	18.13	−98.38
		INT3	−177.24	5.35	−60.38
3	MD 800 ps	INT1	−362.24	−89.86	−150.47
		INT2	−264.07	7.41	−113.97
		INT3	−166.66	3.71	−66.90
1−3	average[b]	INT1	−354.93	−65.78	−175.96
		INT2	−281.40	14.51	−108.48
		INT3	−174.26	5.59	−62.96
1−3	standard deviation[c]	INT1	11.73	17.37	20.10
		INT2	15.03	5.02	7.15
		INT3	5.41	1.65	2.83

[a] Energies (in kcal/mol) are calculated at the MP2/6-31G level. INT1, 2, and 3 are RXR−SRC1, AF2C−SRC1, and AF2C−LXXLL interactions, respectively. Interaction energies of the N- and C-terminal residues are not included. [b] Average of the samples 1−3. [c] Standard deviation of the samples 1−3.

kcal/mol, respectively, by the MM-GBSA method. These results of the MM calculations indicate that, if the effects of solvent and entropy are included in the FMO calculations, the SRC1 binding energies calculated by the FMO method would be substantially reduced, while the qualitative tendency of the SRC1 binding affinities for RXR would not be changed. However, it is noted that the difference between E453K and E456K in the SRC1 binding affinities is small. Therefore, in the next section, we attempt to clarify what measure better correlates with the degree of the transcriptional activation through the examinations of molecular interactions and CTs at the residue level, which can be appropriately described by the FMO calculations.

3.3. Receptor−Coactivator Interaction Energies. To examine the influence of mutations in AF2C on the RXR−SRC1 interaction, the total IFIEs of whole RXR with the whole SRC1 (INT1) were calculated by the FMO method at the MP2/6-31G level as shown in Table 2. The total IFIEs of AF2C with the whole SRC1 (INT2) and those of AF2C with the LXXLL motif (INT3) were also calculated to investigate the components of the RXR−SRC1 interaction in detail. Note that the electrostatic interaction energies between the dissociated N- and C-terminal residues of SRC1 and charged residues of RXR could be one of the reasons for the overestimation of interaction energies between RXR and SRC1 since the N- and C-terminal residues in the model system are not ends of the peptide chains in the actual system. Hence, in this section, the IFIEs between the RXR residues and the SRC1 residues except for the N- and C-terminal residues of RXR and SRC1 are discussed.

So as to confirm the validity of the canonical MP2 calculation for the receptor−coactivator interaction energies, the SCS-MP2 and SOS-MP2 calculations for the interaction energies were also performed. The tendency of the receptor−coactivator interaction energies estimated by the canonical MP2 method was similar to that estimated by the SCS-MP2 and SOS-MP2 methods, though the attractive and repulsive interaction energies were somewhat overestimated and underestimated, respectively, by the canonical MP2 method. For example, the magnitudes of the RXR−SRC1 interaction energies (INT1) calculated for sample 1 are in order of WT > E456K > E453K with the calculated values of −364.2, −199.6, and −58.0 kcal/mol at the MP2/6-31G level, respectively, as shown in Table 2, while those are also in order of WT > E456K > E453K by the SCS-MP2 and SOC-MP2 calculations with the calculated values of −353.7, −190.5, and −52.3 kcal/mol at the SCS-MP2/6-31G level and −348.4, −186.0, and −49.4 kcal/mol at the SOS-MP2/6-31G level, respectively. Hence, following discussions are based on the results of the canonical MP2 calculations.

As shown in Table 2, the average magnitude of the RXR−SRC1 interaction energy (INT1), which does not include the interaction energies of the N- and C-terminal residues, of WT prepared by the MD simulation is almost the same as that of WT of the X-ray crystal structure. Therefore, it is indicated that, as discussed in the previous section, the average magnitude of the coactivator binding energy (ΔE calculated by the FMO method; Table 1) of WT prepared by the MD simulation was calculated somewhat larger than that of WT of the X-ray crystal structure, primarily because of the difference in the configurations of the N- and C-terminals of SRC1.

Table 2 shows that the magnitudes of the averages of the RXR−SRC1 interaction energies (INT1) are in order of WT > E456K > E453K. The average of the RXR−SRC1 interaction energies of WT is larger in magnitude than that of E453K and E456K by 289.2 and 179.0 kcal/mol, respectively, and the difference in the RXR−SRC1 interaction energy between E453K and E456K is large. Additionally, the RXR−SRC1 interaction energies of each sample, which corresponds to the snapshots at the same time steps of the MD simulations, are also in order of WT > E456K > E453K, and the difference in the RXR−SRC1 interaction energy between E453K and E456K of each sample is also large. These results indicate that the average strength of the RXR−SRC1 interaction seen in terms of IFIEs well-correlates with the degree of the transcriptional activation (WT > E456K > E453K).[20]

The average values of the RXR−SRC1 (INT1) and AF2C−SRC1 (INT2) interaction energies of WT show that the AF2C−SRC1 interaction holds most (79%) of the RXR−SRC1 interaction, indicating that the AF2C−SRC1 interaction significantly contributes to the coactivator binding. A remarkable difference between WT, E453K, and E456K appeared in the AF2C−SRC1 interaction. It is noteworthy that the AF2C−SRC1 interaction energies of WT and E456K are attractive, but only the AF2C−SRC1 interaction energy of E453K is repulsive in each sample and the average. A similar tendency was observed in the AF2C−LXXLL interaction; that is, the AF2C−LXXLL interaction energies of WT and E456K are attractive, but only the AF2C−LXXLL interaction energy of E453K is repulsive in each sample and the average. These results indicate that, in E453K, the RXR−SRC1 interaction is substantially inhibited by the repulsive interaction between AF2C and SRC1 including the LXXLL motif.

In order to clarify why the interaction between AF2C and SRC1 including the LXXLL motif is repulsive only in E453K, the AF2C−SRC1 and AF2C−LXXLL interactions were analyzed in detail at the residue level. The IFIEs and distances between AF2C and SRC1 residues calculated for WT, E453K, and E456K of sample 1 are shown in Table 3A,B,C, respectively, while similar features were observed in samples 1, 2, and 3 in common. Totals 1 and 2 of Table 3A,B,C are the total IFIEs of the AF2C−LXXLL and AF2C−SRC1 interaction energies, respectively. The distances between the Cα atoms of AF2C and those of SRC1 are also shown in Table 3A,B,C. Averages 1 and 2 of Table 3A,B,C are the average Cα−Cα distances between AF2C and LXXLL and those between AF2C

TABLE 3: IFIEs and Distances between RXR and SRC1 Residues Calculated for (A) WT, (B) E453K, and (C) E456K of Sample 1[a]

		(A) RXR[b]							
		H3	AF2C						
	SRC1[c]	Lys284	Phe450	Leu451	Met452	Glu453	Met454	Leu455	Glu456
IFIE	Lys631	17.17	−4.51	0.96	0.87	−53.14	1.74	1.86	−29.07
	Ile632	−1.52	−4.43	0.22	0.32	−30.04	0.94	0.50	−2.68
	Leu633	−3.95	−2.73	−0.20	0.10	−27.40	−0.46	0.36	−1.84
	His634	21.87	−1.93	−1.64	0.13	−51.38	−1.29	1.65	−25.59
	Arg635	31.71	−1.89	0.45	0.88	−38.57	0.66	1.54	−19.29
	Leu636	−2.47	−1.02	−0.10	0.02	−3.90	0.01	0.14	−1.05
	Leu637	−34.59	−0.37	−0.04	0.06	−3.48	0.11	0.15	−0.99
	Gln638	5.62	−0.22	−0.11	0.10	−4.12	0.06	0.25	−1.35
	total1[d]	12.57	−7.94	−1.53	1.21	−124.72	−0.97	3.84	−48.76
	total2[e]	33.84	−17.09	−0.45	2.49	−212.02	1.76	6.45	−81.86
distance[f]	Lys631	17.00	8.73	11.64	10.66	7.88	11.14	14.16	14.43
	Ile632	14.68	6.65	9.93	10.24	7.87	10.67	13.70	14.97
	Leu633	11.83	7.90	10.00	10.76	7.55	9.12	12.72	13.96
	His634	12.43	11.26	13.60	13.69	10.19	12.02	15.74	16.25
	Arg635	12.36	11.61	14.62	15.17	12.25	14.44	17.94	18.98
	Leu636	9.30	11.06	13.62	15.13	12.45	13.85	17.28	18.97
	Leu637	6.97	13.39	15.28	16.66	13.44	14.12	17.84	19.16
	Gln638	8.48	16.18	18.55	19.75	16.56	17.70	21.43	22.60
	average1[g]	10.58	11.04	13.42	14.28	11.18	12.71	16.31	17.46
	average2[h]	11.63	10.85	13.41	14.01	11.02	12.88	16.35	17.42

		(B) RXR[b]							
		H3	AF2C						
	SRC1[c]	Lys284	Phe450	Leu451	Met452	Lys453	Met454	Leu455	Glu456
IFIE	Lys631	18.45	−1.27	0.36	0.76	31.78	−0.64	0.89	−23.13
	Ile632	−1.10	−1.54	0.23	0.19	2.63	0.02	0.15	−1.05
	Leu633	−2.64	−1.81	−0.03	0.00	3.08	−0.03	0.06	−0.79
	His634	22.94	−2.56	−0.77	0.30	27.05	−1.87	0.81	−27.52
	Arg635	33.20	−0.63	0.74	1.25	30.44	−0.47	1.07	−20.90
	Leu636	−1.44	−0.19	−0.03	0.01	1.03	−0.06	0.04	−0.80
	Leu637	−35.93	−0.31	0.01	0.06	1.51	−0.10	0.08	−0.96
	Gln638	5.54	−0.13	−0.02	0.12	2.23	−0.11	0.15	−1.33
	total1[d]	16.13	−5.50	−0.08	1.62	63.11	−2.53	2.07	−50.97
	total2[e]	39.02	−8.43	0.48	2.69	99.75	−3.26	3.26	−76.49
distance[f]	Lys631	17.02	10.96	14.37	14.85	11.75	13.79	16.25	14.33
	Ile632	15.21	8.68	12.12	13.45	11.01	12.76	15.80	14.79
	Leu633	12.20	9.01	11.59	13.32	10.53	11.13	14.50	13.71
	His634	12.33	12.64	15.34	16.70	13.53	14.21	17.26	15.81
	Arg635	12.50	13.21	16.24	18.02	15.37	16.38	19.66	18.55
	Leu636	9.53	12.35	14.76	17.24	15.03	15.32	18.97	18.60
	Leu637	7.17	14.41	16.35	18.69	16.06	15.70	19.25	18.69
	Gln638	8.77	17.33	19.68	21.93	19.24	19.30	22.78	21.91
	average1[g]	10.75	12.32	14.85	16.79	14.10	14.55	17.93	17.07
	average2[h]	11.84	12.32	15.05	16.77	14.06	14.82	18.06	17.05

		(C) RXR[b]							
		H3	AF2C						
	SRC1[c]	Lys284	Phe450	Leu451	Met452	Glu453	Met454	Leu455	Lys456
IFIE	Lys631	16.17	−0.90	1.43	−0.77	−65.07	2.58	2.19	32.20
	Ile632	0.34	−3.91	1.42	−0.11	−24.08	0.09	0.30	2.61
	Leu633	−1.85	−2.08	−0.49	−0.07	−21.12	−1.93	0.48	2.00
	His634	19.78	−2.47	−0.49	0.12	−45.06	−0.90	1.15	22.27
	Arg635	29.23	0.02	1.64	1.54	−32.02	0.90	1.46	19.51
	Leu636	−0.58	−1.81	−0.33	−0.23	−1.69	−0.23	−0.09	0.38
	Leu637	−12.21	−0.55	0.02	−0.03	−1.97	−0.17	0.09	0.57
	Gln638	−0.93	0.07	0.08	0.12	−0.06	0.09	0.08	0.14
	total1[d]	34.37	−6.90	0.35	1.33	−101.87	−2.34	3.09	44.73
	total2[e]	49.96	−11.63	3.28	0.58	−191.08	0.42	5.65	79.69
distance[f]	Lys631	21.54	8.18	11.26	9.73	7.66	10.97	13.19	12.12
	Ile632	18.06	6.13	9.84	9.73	7.74	9.99	12.97	12.88
	Leu633	15.60	6.89	9.96	10.23	7.20	8.37	11.91	11.68
	His634	15.84	10.42	13.76	13.90	10.82	12.18	15.68	15.04
	Arg635	14.62	10.00	13.65	14.54	12.24	13.35	16.94	17.08
	Leu636	11.13	9.37	12.47	14.28	12.19	12.15	15.94	16.77
	Leu637	8.91	13.15	16.02	17.94	15.60	15.20	19.07	19.79
	Gln638	11.85	15.53	18.82	20.34	17.91	18.17	22.00	22.34
	average1[g]	13.22	9.97	13.17	14.18	11.61	12.25	15.91	16.07
	average2[h]	14.69	9.96	13.22	13.83	11.42	12.55	15.96	15.96

[a] Energies (in kcal/mol) are calculated at the MP2/6-31G level. Sample 1 is obtained from the snapshot at 1 ns of the MD simulation. [b] All AF2C residues (Phe450−Glu456) and one of the charge clamp in H3 (Lys284) are listed. [c] All SRC1 residues except for N- and C-terminal residues are listed. [d] Sum of IFIEs between each RXR residue and LXXLL motif in SRC1. [e] Sum of IFIEs between each RXR residue and all listed SRC1 resides. [f] Cα−Cα distances (in Å) of main chains in RXR and SRC1. [g] Average of Cα−Cα distances between each RXR residue and LXXLL motif in SRC1. [h] Average of Cα−Cα distances between each RXR residue and all listed SRC1 resides.

TABLE 4: Charge Changes (Δq)[a] of Receptor (R), Ligand (L), and Coactivator (C) Calculated for WT, E453K, and E456K

			WT			E453K			E456K		
sample			q_1	q_2	Δq	q_1	q_2	Δq	q_1	q_2	Δq
0	crystal structure	R	−0.05	−0.32	0.27						
		L	−0.69	−0.68	−0.01						
		C	2.74	3.00	−0.26						
1	MD 1 ns	R	−0.11	−0.35	0.24	1.65	1.64	0.01	2.11	1.67	0.44
		L	−0.66	−0.65	−0.01	−0.65	−0.64	−0.01	−0.67	−0.67	−0.01
		C	2.77	3.00	−0.23	3.00	3.00	0.00	2.56	3.00	−0.44
2	MD 900 ps	R	−0.02	−0.35	0.33	1.68	1.67	0.01	2.05	1.67	0.38
		L	−0.66	−0.65	−0.01	−0.67	−0.67	−0.01	−0.68	−0.67	−0.01
		C	2.68	3.00	−0.32	3.00	3.00	0.00	2.63	3.00	−0.37
3	MD 800 ps	R	−0.05	−0.34	0.29	1.84	1.66	0.18	2.08	1.65	0.43
		L	−0.67	−0.66	−0.01	−0.67	−0.66	−0.01	−0.66	−0.65	−0.01
		C	2.72	3.00	−0.28	2.83	3.00	−0.17	2.58	3.00	−0.42
1−3	average[b]	R	−0.06	−0.34	0.28	1.72	1.65	0.07	2.08	1.66	0.42
		L	−0.66	−0.66	−0.01	−0.66	−0.65	−0.01	−0.67	−0.66	−0.01
		C	2.72	3.00	−0.28	2.94	3.00	−0.06	2.59	3.00	−0.41
1−3	standard deviation[c]	R	0.04	0.01	0.04	0.08	0.01	0.08	0.03	0.01	0.03
		L	0.01	0.01	0.00	0.01	0.01	0.00	0.01	0.01	0.00
		C	0.04	0.00	0.04	0.08	0.00	0.08	0.03	0.00	0.03

[a] $\Delta q = q_1 - q_2$. $q_1 = q$(RLC) and $q_2 = q$(RL) + q(C), where q(RLC), q(RL), and q(C) are the total charges of the receptor−ligand−coactivator complex (RLC), the receptor−ligand complex (RL), and the coactivator (C), respectively. Charges (in atomic units) are calculated at the MP2/6-31G level. [b] Average of the samples 1−3. [c] Standard deviation of the samples 1−3.

and SRC1, respectively. The LXXLL motif of SRC1 is formed by Leu633, His634, Arg635, Leu636, and Leu637. In this section, the results of the IFIEs and distances of the AF2C−SRC1 interactions are discussed, since the results of the IFIEs and distances of the AF2C−LXXLL interactions are similar to those of the AF2C−SRC1 interactions, as shown in Table 3A,B,C.

As shown in Table 3A, two charged residues Glu453 and Glu456 of AF2C in WT have larger attractive interaction energies with SRC1 than the hydrophobic residues. In WT, the average Cα−Cα distance between Glu453 and SRC1 is shorter than that between Glu456 and SRC1 by 6.40 Å (average 2), and accordingly, the total energy of the interaction between Glu453 and SRC1 is larger in magnitude than that between Glu456 and SRC1 by 130.2 kcal/mol (total 2). Both of the large attractive interaction energies of Glu453 and Glu456 with SRC1 lead to the attractive AF2C−SRC1 interaction, and consequently, lead to the strong RXR−SRC1 interaction in WT.

On the other hand, in E453K, as shown in Table 3B, the average Cα−Cα distance between the substituted residue Lys453 and SRC1 is shorter than that between Glu456 and SRC1 by 2.99 Å (average 2), and the total energy of the repulsive interaction between Lys453 and SRC1 is larger in magnitude than that of the attractive interaction between Glu456 and SRC1 by 23.3 kcal/mol (total 2). The large repulsive interaction energy of Lys453 with SRC1 leads to the repulsive AF2C−SRC1 and, consequently, leads to the weak RXR−SRC1 interaction in E453K. In E456K, as shown in Table 3C, the average Cα−Cα distance between Glu453 and SRC1 is shorter than that between the substituted residue Lys456 and SRC1 by 4.54 Å (average 2), and the total energy of the attractive interaction between Glu453 and SRC1 is larger in magnitude than that of the repulsive interaction between Lys456 and SRC1 by 111.4 kcal/mol (total 2). The large attractive interaction energy of Glu453 with SRC1 leads to the attractive AF2C−SRC1 and RXR−SRC1 interactions in E456K. These results indicate that the mutation of Glu453 has a greater effect on the inhibition of the AF2C−SRC1 interaction than the mutation of Glu456 and, thus, impairs the RXR−SRC1 interaction more severely than the mutation of Glu456.

3.4. Charge Transfers on the Coactivator Binding. The influence of mutations in AF2C on the CTs on the coactivator binding was also analyzed by the calculations of the Mulliken atomic charges of RXR, 9cRA, and SRC1 at the MP2/6-31G level as shown in Table 4. The charge changes (Δq) on the coactivator binding are given as follows,

$$\Delta q = q(\mathrm{RLC}) - [q(\mathrm{RL}) + q(\mathrm{C})] \quad (5)$$

where q(RLC), q(RL), and q(C) are the Mulliken atomic charges of the receptor−ligand−coactivator complex (RLC), the receptor−ligand complex (RL), and the coactivator (C), respectively. As we have mentioned above, the charges of individual RXR of WT, E453K and E456K are 0e, +2e, and +2e, respectively, and the charges of individual 9cRA and SRC1 are −1e and +3e, respectively. The total charges of WT, E453K, and E456K complexes are +2e, +4e, and +4e, respectively. On the basis of the previous QM studies[29,30] on ER, it was suggested that the differences between the charge distributions of each residue of the receptors with and without the ligand binding reflected CT interactions between the ligand and each residue. Hence, in this section, the CTs are discussed on the basis of the differences between the charge distributions of the receptors with and without the coactivator binding.

The charge changes Δq calculated for the samples of WT show that the charges of RXR increase by 0.24∼0.33e and almost equal amounts of negative charges are induced on SRC1 by −0.23∼−0.32e, whereas the charges of 9cRA are nearly constant. The average charge change Δq calculated for WT also shows that the charge of RXR increases by 0.28e and equal amount of negative charge is induced on SRC1 by −0.28e. These results indicate that CT (electron transfer) occurs from RXR to SRC1 in WT on the coactivator binding. On one hand, the average Δq calculated for E453K shows that the charge of RXR increases by 0.07e, and almost the same amount of negative charge is induced on SRC1 by −0.06e, indicating that CT in E453K occurs from RXR to SRC1; however, the amount of CT in E453K is smaller than that in WT. On the other hand, the average Δq calculated for E456K shows that the charge of RXR increases by 0.42e, and almost the same amount of negative charge is induced on SRC1 by −0.41e, indicating that CT occurs from RXR to SRC1; however, the amount of CT in

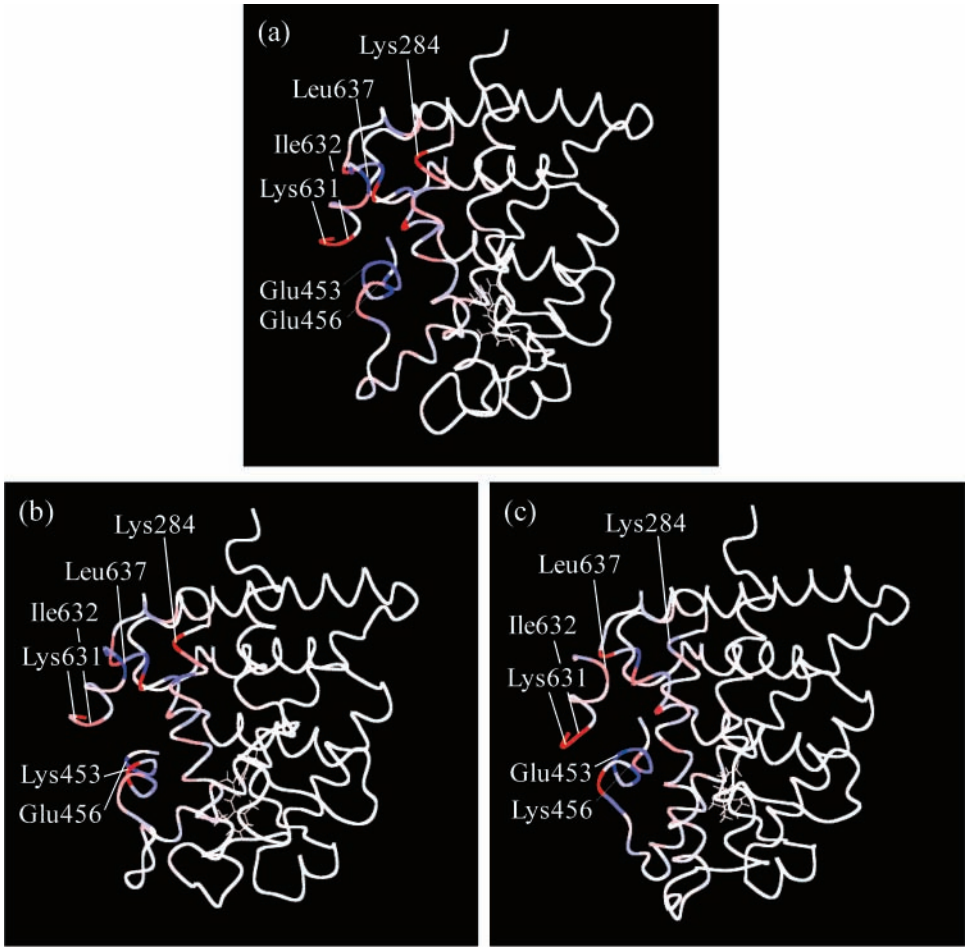

Figure 4. Visualizations of the charge changes Δq of (a) WT, (b) E453K, and (c) E456K calculated at the MP2/6-31G level; $\Delta q = q(\mathrm{RLC}) - [q(\mathrm{RL}) + q(\mathrm{C})]$. The positive and negative charge changes are colored in blue and red, respectively.

E456K is larger than that in WT. These results point out that the CTs in E453K and E456K are somewhat different from the CT in WT.

In order to clarify why the CTs in E453K and E456K are different from the CT in WT, these different types of CTs were analyzed in detail at the residue level. The visualized charge changes Δq for WT, E453K, and E456K of sample 1 are shown in Figure 4a−c, respectively, while similar features were observed in samples 1, 2, and 3 in common. The positive and negative charge changes are colored in blue and red, respectively, and the magnitudes of the charge differences are represented by the deepness of hue. The Δq values of all residues of AF2C in RXR and of SRC1 calculated for WT, E453K, and E456K of sample 1 are shown in Table 5. The Δq values of Lys284 in H3, which forms the "charge clamp" with Glu453 in H12, are also shown in Table 5. In addition, the differences between charge changes Δq of E453K and WT and those between charge changes Δq of E456K and WT are also shown in Table 5 as $\Delta\Delta q_1$ and $\Delta\Delta q_2$, respectively. Here, the charge differences ($\Delta\Delta q_1$ and $\Delta\Delta q_2$) are given as follows,

$$\Delta\Delta q_1 = \Delta q(\mathrm{E453K}) - \Delta q(\mathrm{WT}) \quad (6)$$

$$\Delta\Delta q_2 = \Delta q(\mathrm{E456K}) - \Delta q(\mathrm{WT}) \quad (7)$$

Figure 4a−c shows that the residues of SRC1 and its binding site of RXR including AF2C and the "charge clamp" are colored in red or blue. Table 5 shows that the absolute values of the total charge changes Δq of the listed residues of RXR including AF2C and the "charge clamp" (total 1) are nearly equal to those of SRC1 (total 2). Thus, Figure 4a−c and Table 5 indicate that the CTs in all of WT, E453K, and E456K mainly occur between the listed residues of RXR and SRC1.

As shown in Table 5, in the CT of WT, positive charge changes Δq of the residues in RXR exceed negative charge changes Δq of the residues in RXR by about $0.2e$ (total 1), and negative charge changes Δq of the residues in SRC1 exceed positive charge changes Δq of the residues in SRC1 by about $0.2e$ (total 2). In particular, large positive charge changes Δq are observed at Leu451, Glu453, Met454, Leu455, and Glu456 in AF2C of RXR with the calculated values greater than $0.05e$, and large negative charge changes Δq are observed at His630, Lys631, and Ile632 in SRC1 with the calculated values lower than $-0.05e$, showing that the CT from RXR to SRC1 occurs mainly from these five residues in AF2C of RXR to these three residues of SRC1. In addition, a large negative charge change Δq is seen at Lys284 in H3 of RXR with the calculated value of $-0.11e$, and large positive charge changes Δq are seen at Leu637 and Glu639 in SRC1 with the calculated values of $0.08e$, showing that the CT from SRC1 to RXR occurs mainly from this residue in H3 of RXR to these two residues of SRC1. In the following, the charge changes of the residues of RXR and SRC1 except for those of N- and C-terminal residues of SRC1 are discussed, since the N- and C-terminal residues in the model system are not ends of the peptide chains in the actual system.

TABLE 5: Charge Differences of Residues Calculated for WT, E453K, and E456K of Sample 1[a]

			Δq			difference[b]	
	position	residue	WT	E453K	E456K	$\Delta\Delta q_1$	$\Delta\Delta q_2$
RXR	H3	Lys284	−0.11	−0.16	0.03	−0.04	0.15
	AF2C	Phe450	−0.03	−0.04	0.01	0.00	0.05
		Leu451	0.08	0.04	0.07	−0.04	−0.01
		Met452	0.03	0.03	0.03	0.00	0.00
		Glu453	0.06	−0.10	0.23	−0.16	0.17
		Met454	0.06	0.02	0.06	−0.04	−0.01
		Leu455	0.05	0.05	0.05	0.00	0.00
		Glu456	0.07	0.08	−0.04	0.01	−0.11
		total1[c]	0.20	−0.06	0.43	−0.27	0.23
SRC1	N-terminus	His630	−0.19	−0.13	−0.20	0.06	−0.01
		Lys631	−0.13	−0.03	−0.12	0.10	0.00
		Ile632	−0.08	−0.05	−0.08	0.03	0.00
		Leu633	0.01	0.01	0.02	0.01	0.01
		His634	0.04	0.03	0.01	−0.01	−0.03
		Arg635	−0.03	−0.01	−0.02	0.01	0.00
		Leu636	−0.04	−0.02	−0.01	0.03	0.03
		Leu637	0.08	0.08	−0.04	−0.01	−0.12
		Gln638	0.02	0.04	0.03	0.02	0.01
	C-terminus	Glu639	0.08	0.07	−0.02	−0.01	−0.10
		total2[d]	−0.23	0.00	−0.44	0.23	−0.20

[a] $\Delta q = q(\mathrm{RLC}) - [q(\mathrm{RL}) + q(\mathrm{C})]$, where q(RLC), q(RL), and q(C) are the total charges of the receptor−ligand−coactivator complex (RLC), the receptor−ligand complex (RL), and the coactivator (C), respectively. Charges (in atomic units) are calculated at the MP2/6-31G level. Sample 1 is obtained from the snapshot at 1 ns of the MD simulation. Glu453 and Glu456 are substituted by Lys in E453K and E456K, respectively. [b] $\Delta\Delta q_1 = q(\mathrm{E453K}) - q(\mathrm{WT})$, $\Delta\Delta q_2 = q(\mathrm{E456K}) - q(\mathrm{WT})$. [c] Sum of all listed RXR residues. [d] Sum of all listed SRC1 residues.

It is noteworthy, as shown in Figure 4a, that Glu453 and Lys284 of the "charge clamp" in WT are colored in dark-blue and dark-red, with the large positive and negative charge changes, respectively, while Lys631 and Ile632 of SRC1, which are situated near Glu453, and Leu637 of SRC1, which is situated near Lys284, are colored in dark-red and dark-blue, with the large negative and positive charge changes, respectively. The calculated Cα−Cα distances from Glu453 to Lys631 and Ile632 are 7.88 and 7.87 Å, respectively, and that from Lys284 to Leu637 is 6.97 Å (Table 3A). Additionally, the side chain carbonyl of Glu453 forms hydrogen bonds with the main chain amides of Lys631 and Ile632 with the calculated O−H distances of 3.09 and 1.97 Å, respectively. Besides, Glu453 has large attractive interaction energies of −53.1 and −30.0 kcal/mol with Lys631 and Ile632, respectively, and Lys284 has a large interaction energy of −34.6 kcal/mol with Leu637 (Table 3A). These results indicate that electrons could transfer from Glu453 to Lys631 and Ile632 in the electron donation from RXR to SRC1, and electrons could transfer from Leu637 to Lys284 in the electron back-donation from SRC1 to RXR. From these results, it is suggested that the CT from RXR to SRC1 occurs through the electron donation and electron back-donation via the "charge clamp" in WT. It is also suggested that, in WT, the larger electron donation from RXR to SRC1 rather than the electron back-donation from SRC1 to RXR results in the CT from RXR to SRC1 in total, since the positive and negative charge changes in RXR and SRC1, respectively, exceed the negative and positive charge changes in RXR and SRC1, respectively, as mentioned above.

In a comparison of Figure 4b with Figure 4a, the color of the substituted residue Lys453 in E453K is different from that of Glu453 in WT. Lys453 in E453K is colored in dark-red with the large negative charge change Δq of −0.10e, whereas Glu453 in WT is colored in dark-blue with the large positive charge change Δq of 0.06e. The opposite charge changes were observed at Lys453 in E453K and at Glu453 in WT, because the Lys453 and Glu453 are basic and acidic amino acid residues, respectively. At the same time as this difference appears, Lys631 and Ile632 of SRC1 in E453K are colored in light-red with the small negative charge changes Δq of −0.03e and −0.05e, respectively, whereas these residues in WT are colored in dark-red with the large negative charge changes Δq of −0.13e and −0.08e. Accordingly, the largest negative difference $\Delta\Delta q_1$ of −0.16e is calculated at Glu453 in the listed RXR residues, and the positive differences $\Delta\Delta q_1$ of 0.10e and 0.03e are calculated at Lys631 and Ile632 in the SRC1 residues, as shown in Table 5. Besides, the interactions of Lys453 with Lys631 and Ile632 in E453K are repulsive with the calculated energies of 31.8 and 2.6 kcal/mol, respectively (Table 3B), whereas the interactions of Glu453 with Lys631 and Ile632 in WT are attractive with the calculated energies of −53.1 and −30.0 kcal/mol, respectively (Table 3A). These results indicate that the electron donation to Lys631 and Ile632 would be reduced because of the charge redistribution of Lys453 in E453K. Therefore, it is suggested that, in E453K, the CT from RXR to SRC1 is inhibited, because the electron donation from RXR to SRC1 is reduced, especially at the substituted residue Lys453.

In a comparison of Figure 4c with Figure 4a, the color of Lys284 in E456K is different from that in WT. Lys284 in E453K is colored in light-blue with the small positive charge change Δq of 0.03e, whereas Lys284 in WT is colored in dark-red with the large negative charge change Δq of −0.11e. At the same time as this difference appears, Lys637 of SRC1 in E456K is colored in light-red with the small negative charge change Δq of −0.04e, whereas this residue in WT is colored in dark-blue with the large positive charge change Δq of 0.08e. Thus, the large positive difference $\Delta\Delta q_2$ of 0.15e is calculated at Lys284 in the listed RXR residues, and the largest negative difference $\Delta\Delta q_2$ of −0.12e is calculated at Leu637 in the SRC1 residues, as shown in Table 5. In addition, the Cα−Cα distance from Lys284 to Leu637 in E456K (8.91 Å; Table 3C) is longer than that in WT (6.97 Å; Table 3A) by 1.94 Å. It is shown that, because the distance between Lys284 and Leu637 in E456K are longer than that in WT and the conformation of these residues in E456K is different from that in WT, the different charge changes were observed at these residues in E456K and WT. Besides, the attractive interaction energy between Lys284 and Leu637 in E456K (−12.2 kcal/mol; Table 3C) is smaller in magnitude than that in WT (−34.6 kcal/mol; Table 3A) by 22.4 kcal/mol. These results indicate that the electron back-donation from Leu637 would be reduced because of the charge redistribution of Lys284 in E456K. Hence, it is suggested that, in E456K, the excessive CT from RXR to SRC1 occurs, because the electron back-donation from SRC1 to RXR is reduced, especially at Lys284.

Considering the results of the CTs and interaction energies in WT, E453K, and E456K altogether, it is indicated that the reductions of the electron donation or back-donation between the RXR and the SRC1 residues are associated with the inhibitions of the interactions between the RXR and the SRC1 residues. Furthermore, the charge changes $\Delta\Delta q_1$ and $\Delta\Delta q_2$ of −0.16e and −0.11e calculated for the mutations of Glu453 and Glu456, respectively, show that the electron donation from RXR to SRC1 is more effectively impaired by the mutation of Glu453 than by that of Glu456. Correspondingly, the interaction between RXR and SRC1 is more severely impaired by the mutation of Glu453 than by that of Glu456 as mentioned above. Our results

suggest that the CT from RXR to SRC1 might play an important supportive role for the interaction between RXR and SRC1.

4. Conclusions

The ab initio FMO calculations were performed for RXR complexes with its ligand 9cRA and coactivator SRC1 to examine the influence of mutations in AF2C of RXR on molecular interactions between 9cRA liganded RXR and SRC1 coactivator. The RXR−SRC1 interactions in three types of RXR-9cRA-SRC1 complexes, namely, WT, E453K, E456K, were compared. Through the comparison of these three complexes, possible causes for a marked decrease in the transcriptional activity of RXR by the mutation of the highly conserved charged residue Glu453 of AF2C[20] were discussed.

It was quantitatively demonstrated that the strength of the RXR−SRC1 interaction well correlates with the degree of the transcriptional activation (WT > E456K > E453K).[20] In WT, the AF2C−SRC1 interaction was proved to hold most (79%) of the RXR−SRC1 interaction, indicating that the AF2C−SRC1 interaction significantly contributes to the coactivator binding. A remarkable difference between the three types of RXR-9cRA-SRC1 complexes appeared in the AF2C−SRC1 interaction, where each AF2C−SRC1 interaction of WT and E456K is attractive, but that of E453K is repulsive. In E453K, the RXR−SRC1 interaction was found to be substantially inhibited by the AF2C−SRC1 repulsive interaction, especially at the substituted residue Lys453.

In addition, it was found that different patterns of CTs occur in the three types of RXR-9cRA-SRC1 complexes on the coactivator binding. It was also found that the charge changes at Glu453 and Lys284 of the "charge clamp" are profoundly concerned with the electron donation from RXR to SRC1 and the electron back-donation from SRC1 to RXR, where Glu453 and Lys284 play roles as an electron donor to SRC1 and an electron acceptor from SRC1, respectively. In WT, the CT from RXR to SRC1 was proved to occur, which is considered to be caused by the larger electron donation from RXR to SRC1 than by the electron back-donation from SRC1 to RXR. The electron donation in WT was mainly observed from AF2C to SRC1. On the other hand, in E453K, the CT from RXR to SRC1 was found to be inhibited by the decreased electron donation from AF2C to SRC1, especially at the substituted residue Lys453.

Taken together, our findings suggest that the inhibitions of the local RXR−SRC1 interaction via AF2C and of the local CT from RXR to SRC1 via AF2C would be the possible causes for the marked decrease in the transcriptional activity of RXR by the mutation of the highly conserved charged residue Glu453 of AF2C. To obtain a more reliable understanding of these molecular interactions and CTs, structures of model complexes should be prepared by relaxations and optimizations in aqueous solution using QM methods, and effects of solvent and entropy should be included in QM calculations in future studies. However, we suppose that the QM calculations based on the FMO method could provide us with useful information about the molecular interactions and CTs upon the coactivator binding at the residue level and that the knowledge obtained from this work would be helpful for our better understanding of the transcriptional activation mechanism of RXR and related NRs.

Acknowledgment. We thank Dr. Yuto Komeiji for helpful comments on MD calculations, and Dr. Takeshi Ishikawa and Dr. Hirofumi Watanabe for technical assistance. This work was supported by the "Core Research for Evolutional Science and Technology" (CREST) project of the Japan Science and Technology Agency.

Supporting Information Available: Root-mean-squared deviation (RMSD) measurements of the MD simulations. This material is available free of charge via the Internet at http://pubs.acs.org.

References and Notes

(1) Ross, S. A.; McCaffery, P. J.; Drager, U. C.; Luca, L. M. D. *Physiol. Rev.* **2000**, *80*, 1021−1054.

(2) Miles, S. A.; Dezube, B. J.; Lee, J. Y.; Krown, S. E.; Fletcher, M. A.; Saville, M. W.; Kaplan, L.; Groopman, J.; Scadden, D. T.; Cooley, T.; Von Roenn, J.; Friedman-Kien, A. *AIDS* **2002**, *16*, 421−429.

(3) Mangelsdorf, D. J.; Thummel, C.; Beato, M.; Herrlich, P.; Schütz, G.; Umesono, K.; Blumberg, B.; Kastner, P.; Mark, M.; Chambon, P.; Evans, R. M. *Cell* **1995**, *83*, 835−839.

(4) Nagy, L.; Schwabe, J. W. *Trends Biochem. Sci.* **2004**, *29*, 317−324.

(5) Bourguet, W.; Ruff, M.; Chambon, P.; Gronemeyer, H.; Moras, D. *Nature* **1995**, *375*, 377−382.

(6) Renaud, J. P.; Rochel, N.; Ruff, M.; Vivat, V.; Chambon, P.; Gronemeyer, H.; Moras, D. *Nature* **1995**, *378*, 681−689.

(7) Egea, P. F.; Mitschler, A.; Rochel, N.; Ruff, M.; Chambon, P.; Moras, D. *EMBO J.* **2000**, *19*, 2592−2601.

(8) Moras, D.; Gronemeyer, H. *Curr. Opin. Cell. Biol.* **1998**, *10*, 384−391.

(9) Nolte, R. T.; Wisely, G. B.; Westin, S.; Cobb, J. E.; Lambert, M. H.; Kurokawa, R.; Rosenfeld, M. G.; Willson, T. M.; Glass, C. K.; Milburn, M. V. *Nature* **1998**, *395*, 137−143.

(10) Darimont, B. D.; Wagner, R. L.; Apriletti, J. W.; Stallcup, M. R.; Kushner, P. J.; Baxter, J. D.; Fletterick, R. J.; Yamamoto, K. R. *Genes Dev.* **1998**, *12*, 3343−3356.

(11) Gampe, R. T.; Montana, V. G.; Lambert, M. H.; Miller, A. B.; Bledsoe, R. K.; Milburn, M. V.; Kliewer, S. A.; Willson, T. M.; Xu, H. E. *Mol. Cell* **2000**, *5*, 545−555.

(12) Pogenberg, V.; Guichou, J. F.; Vivat-Hannah, V.; Kammerer, S.; Pérez, E.; Germain, P.; Lera, A. R.; Gronemeyer, H.; Royer, C. A.; Bourguet, W. *J. Biol. Chem.* **2005**, *280*, 1625−1633.

(13) Chambon, P. *FASEB J.* **1996**, *10*, 940−954.

(14) Tone, Y.; Collingwood, T. N.; Adams, M.; Chatterjee, V. K. *J. Biol. Chem.* **1994**, *269*, 31157−31161.

(15) Collingwood, T. N.; Rajanayagam, O.; Adams, M.; Wagner, R.; Cavaillès, V.; Kalkhoven, E.; Matthews, C.; Nystrom, E.; Stenlof, K.; Lindstedt, G.; Tisell, L.; Fletterick, R. J.; Parker, M. G.; Chatterjee, V. K. K. *Proc. Natl. Acad. Sci. U.S.A.* **1997**, *94*, 248−253.

(16) Jurutka, P. W.; Hsieh, J.-C.; Remus, L. S.; Whitfield, G. K.; Thompson, P. D.; Haussler, C. A.; Blanco, J. C. G.; Ozato, K.; Haussler, M. R. *J. Biol. Chem.* **1997**, *272*, 14592−14599.

(17) Masuyama, H.; Brownfield, C. M.; St-Arnaud, R.; MacDonald, P. N. *Mol. Endocrinol.* **1997**, *11*, 1507−1517.

(18) Gurnell, M.; Wentworth, J. M.; Agostini, M.; Adams, M.; Collingwood, T. N.; Provenzano, C.; Browne, P. O.; Rajanayagam, O.; Burris, T. P.; Schwabe, J. W.; Lazar, M. A.; Chatterjee, V. K. K. *J. Biol. Chem.* **2000**, *275*, 5754−5759.

(19) Feng, W.; Ribeiro, R. C. J.; Wagner, R. L.; Nguyen, H.; Apriletti, J. W.; Fletterick, R. J.; Baxter, J. D.; Kushner, P. J.; West, B. L. *Science* **1998**, *280*, 1747−1749.

(20) Thompson, P. D.; Remus, L. S.; Hsieh, J. C.; Jurutka, P. W.; Whitfield, G. K.; Galligan, M. A.; Dominguez, C. E.; Haussler, C. A.; Haussler, M. R. *J. Mol. Endocrinol.* **2001**, *27*, 211−227.

(21) Kitaura, K.; Sawai, T.; Asada, T.; Nakano, T.; Uebayasi, M. *Chem. Phys. Lett.* **1999**, *312*, 319−324.

(22) Kitaura, K.; Ikeo, E.; Asada, T.; Nakano, T.; Uebayasi, M. *Chem. Phys. Lett.* **1999**, *313*, 701−706.

(23) Nakano, T.; Kaminuma, T.; Sato, T.; Akiyama, Y.; Uebayasi, M.; Kitaura, K. *Chem. Phys. Lett.* **2000**, *318*, 614−618.

(24) Nakano, T.; Kaminuma, T.; Sato, T.; Fukuzawa, K.; Akiyama, Y.; Uebayasi, M.; Kitaura, K. *Chem. Phys. Lett.* **2002**, *351*, 475−480.

(25) Fedorov, D. G.; Kitaura, K. Theoretical Development of the Fragment Molecular Orbital (FMO) Method. In *Modern Methods for Theoretical Physical Chemistry of Biopolymers*; Starikov, E. B., Lewis, J. B., Tanaka, S., Eds.; Elsevier: Amsterdam, The Netherlands, 2006; pp 3−38.

(26) Nakano, T.; Mochizuki, Y.; Fukuzawa, K.; Amari, S.; Tanaka, S. Developments and Applications of ABINIT-MP Software Based on the Fragment Molecular Orbital Method. In *Modern Methods for Theoretical Physical Chemistry of Biopolymers*; Starikov, E. B., Lewis, J. B., Tanaka, S., Eds.; Elsevier: Amsterdam, The Netherlands, 2006; pp 39−52.

(27) Amari, S.; Aizawa, M.; Zhang, J.; Fukuzawa, K.; Mochizuki, Y.; Iwasawa, Y.; Nakata, K.; Chuman, H.; Nakano, T. *J. Chem. Inf. Model.* **2006**, *46*, 221−230.

(28) Nemoto, T.; Fedorov, D. G.; Uebayasi, M.; Kanazawa, K.; Kitaura, K.; Komeiji, Y. *Comput. Biol. Chem.* **2005**, *29*, 434−439.

(29) Fukuzawa, K.; Kitaura, K.; Uebayasi, M.; Nakata, K.; Kaminuma, T.; Nakano, T. *J. Comput. Chem.* **2005**, *26*, 1−10.
(30) Fukuzawa, K.; Mochizuki, Y.; Tanaka, S.; Kitaura, K; Nakano, T. *J. Phys. Chem. B* **2006**, *110*, 16102−16110, 24276.
(31) Mochizuki, Y.; Nakano, T.; Koikegami, S.; Tanimori, S.; Abe, Y.; Nagashima, U.; Kitaura, K. *Theor. Chem. Acc.* **2004**, *112*, 442−452.
(32) Mochizuki, Y.; Koikegami, S.; Nakano, T.; Amari, S.; Kitaura, K. *Chem. Phys. Lett.* **2004**, *396*, 473−479.
(33) Ito, M.; Fukuzawa, K.; Mochizuki, Y.; Nakano, T.; Tanaka, S. *J. Phys. Chem. B* **2007**, *111*, 3525−3533.
(34) Mochizuki, Y. *Chem. Phys. Lett.* **2005**, *410*, 165−171.
(35) Mochizuki, Y.; Fukuzawa, K.; Kato, A.; Tanaka, S.; Kitaura, K.; Nakano, T. *Chem. Phys. Lett.* **2005**, *410*, 247−253.
(36) Berman, H. M.; Westbrook, J.; Feng, Z.; Gilliland, G.; Bhat, T. N.; Weissig, H.; Shindyalov, I. N.; Bourne, P. E. *Nucleic Acids Res.* **2000**, *28*, 235−242. The RCSB Protein Data Bank (http://www.rcsb.org/).
(37) *MOE*, Version 2005.06; Chemical Computing Group: Montreal, Canada, 2005.
(38) Wang, J.; Cieplak, P.; Kollman, P. A. *J. Comput. Chem.* **2000**, *21*, 1049−1074.
(39) Case, D. A.; Pearlman, D. A.; Caldwell, J. W.; Cheatham, T. E., III; Wang, J.; Ross, W. S.; Simmerling, C. L.; Darden, T. A.; Merz, K. M.; Stanton, R. V.; Cheng, A. L.; Vincent, J. J.; Crowley, M.; Tsui, V.; Gohlke, H.; Radmer, R. J.; Duan, Y.; Pitera, J.; Massova, I.; Seibel, G. L.; Singh, U. C.; Weiner, P. K.; Kollman, P. A. *AMBER 7*; University of California: San Francisco, 2002.
(40) Frisch, M. J.; Trucks, G. W.; Schlegel, H. B.; Scuseria, G. E.; Robb, M. A.; Cheeseman, J. R.; Montgomery, J. A., Jr.; Vreven, T.; Kudin, K. N.; Burant, J. C.; Millam, J. M.; Iyengar, S. S.; Tomasi, J.; Barone, V.; Mennucci, B.; Cossi, M.; Scalmani, G.; Rega, N.; Petersson, G. A.; Nakatsuji, H.; Hada, M.; Ehara, M.; Toyota, K.; Fukuda, R.; Hasegawa, J.; Ishida, M.; Nakajima, T.; Honda, Y.; Kitao, O.; Nakai, H.; Klene, M.; Li, X.; Knox, J. E.; Hratchian, H. P.; Cross, J. B.; Bakken, V.; Adamo, C.; Jaramillo, J.; Gomperts, R.; Stratmann, R. E.; Yazyev, O.; Austin, A. J.; Cammi, R.; Pomelli, C.; Ochterski, J. W.; Ayala, P. Y.; Morokuma, K.; Voth, G. A.; Salvador, P.; Dannenberg, J. J.; Zakrzewski, V. G.; Dapprich, S.; Daniels, A. D.; Strain, M. C.; Farkas, O.; Malick, D. K.; Rabuck, A. D.; Raghavachari, K.; Foresman, J. B.; Ortiz, J. V.; Cui, Q.; Baboul, A. G.; Clifford, S.; Cioslowski, J.; Stefanov, B. B.; Liu, G.; Liashenko, A.; Piskorz, P.; Komaromi, I.; Martin, R. L.; Fox, D. J.; Keith, T.; Al-Laham, M. A.; Peng, C. Y.; Nanayakkara, A.; Challacombe, M.; Gill, P. M. W.; Johnson, B.; Chen, W.; Wong, M. W.; Gonzalez, C.; Pople, J. A. *Gaussian 03*, Revision D.01; Gaussian, Inc.: Wallingford, CT, 2004.
(41) Bayly, C. I.; Cieplak, P.; Cornell, W.; Kollman, P. A. *J. Phys. Chem.* **1993**, *97*, 10269−10280.
(42) Cornell, W. D.; Cieplak, P.; Bayly, C. I.; Kollmann, P. A. *J. Am. Chem. Soc.* **1993**, *115*, 9620−9631.
(43) Cornell, W. D.; Cieplak, P.; Bayly, C. I.; Gould, I. R.; Merz, K. M.; Ferguson, D. M.; Spellmeyer, D. C.; Fox, T.; Caldwell, J. W.; Kollman, P. A. *J. Am. Chem. Soc.* **1995**, *117*, 5179−5197.
(44) Jorgensen, W. L.; Chandrasekhar, J.; Madura, J. D.; Impey, R. W.; Klein, M. L. *J. Chem. Phys.* **1983**, *79*, 926−935.
(45) Berendsen, H. J. C.; Postma, J. P. M.; van Gunsteren, W. F.; DiNola, A.; Haak, J. R. *J. Chem. Phys.* **1984**, *81*, 3684−3690.
(46) Ryckaert, J. P.; Ciccotti, G.; Berendsen, H. J. C. *J. Comput. Phys.* **1977**, *23*, 327−341.
(47) Miyamoto, S.; Kollman, P. A. *J. Comput. Chem.* **1992**, *13*, 952−962.
(48) Essmann, U.; Perera, L.; Berkowitz, M. L.; Darden, T.; Lee, H.; Pedersen, L. G. *J. Chem. Phys.* **1995**, *103*, 8577−8593.
(49) Grimme, S. *J. Chem. Phys.* **2003**, *118*, 9095−9102.
(50) Jung, Y.; Lochan R. C.; Dutoi, A. D.; Head-Gordon, M. *J. Chem. Phys.* **2004**, *121*, 9793−9802.
(51) *ABINIT-MP*, Version 3.0 is available from the website of RSS21 project http://www.rss21.iis.u-tokyo.ac.jp/en.
(52) *BioStation Viewer*, Version 6.00 is available from the website of RSS21 project http://www.rss21.iis.u-tokyo.ac.jp/en.
(53) Tsui, V.; Case, D. A. *Biopolymers* (*Nucl. Acid. Sci.*) **2001**, *56*, 275−291.
(54) Weiser, J.; Shenkin, P. S.; Still, W. C. *J. Comput. Chem.* **1999**, *20*, 217−230.
(55) Massova, I.; Kollman, P. A. *Perspect. Drug Discovery Des.* **2000**, *18*, 113−135.
(56) Case, D. A.; Darden, T. A.; Cheatham, T. E., III; Simmerling, C. L.; Wang, J.; Duke, R. E.; Luo, R.; Merz, K. M.; Wang, B.; Pearlman, D. A.; Crowley, M.; Brozell, S.; Tsui, V.; Gohlke, H.; Mongan, J.; Hornak, V.; Cui, G.; Beroza, P.; Schafmeister, C.; Caldwell, J. W.; Ross, W. S.; Kollman, P. A. *AMBER 8*; University of California: San Francisco, 2004.
(57) van Lipzig, M. M. H.; ter Laak, A. M.; Jongejan, A.; Vermeulen, N. P. E.; Wamelink, M.; Geerke, D.; Meerman, J. H. N. *J. Med. Chem.* **2004**, *47*, 1018−1030.
(58) Šponer, J.; Jurečka, P.; Hobza, P. *J. Am. Chem. Soc.* **2004**, *126*, 10142−10151.
(59) Fukuzawa, K.; Komeiji, Y.; Mochizuki, Y.; Kato, A.; Nakano, T.; Tanaka, S. *J. Comput. Chem.* **2006**, *27*, 948−960.